Effects of aligned fractures on the response of velocity and attenuation ratios to water saturation variation: A laboratory study using synthetic sandstones

Effects of aligned fractures on the response of velocity and attenuation ratios to water saturation variation: A laboratory study using synthetic sandstones

Kelvin Amalokwu[1,2], Angus I. Best[1] and Mark Chapman[3].

[1]*National Oceanography Centre, University of Southampton Waterfront Campus, European Way, Southampton SO*14 3*ZH, United Kingdom.*

[2]*University of Southampton, National Oceanography Centre, Southampton, European Way, Southampton SO*14 3*ZH, United Kingdom*

[3]*University of Edinburgh School of Geosciences, Grant Institute, the King's Building, West Mains Road, Edinburgh EH*9 3*JW, United Kingdom*

Corresponding author e-mail: kelvin.amalokwu@noc.soton.ac.uka

Key words: Seismic anisotropy, Fractures, Fluid saturation, Shear-wave splitting

ABSTRACT

P- to S- wave ratios are important seismic characterisation attributes. Velocity ratios are sensitive to the petrophysical properties of rocks and to the presence of gas. Attenuation ratios have also been shown to be sensitive to the presence of partial liquid/gas saturation. The relationship between liquid/gas saturation and P- and S- wave ratios have been used to distinguish gas saturated rocks from liquid saturated rocks. Aligned fractures are common in the Earth's crust and cause seismic anisotropy and shear wave splitting. However, most existing relationships between partial gas/liquid saturation and P- and S-wave ratios are for non-fractured rocks. We present experimental results comparing the effects of changing water saturation on Q_s/Q_p versus V_p/V_s ratios between a non-fractured rock and one containing fractures aligned parallel to wave propagation direction. We also study the effects of aligned fractures on the response of V_p/V_s to changing water saturation using synthetic fractured sandstones with fractures aligned at 45^o and parallel to wave propagation direction. The results suggest that aligned fractures could have significant effects on the observed trends, some of which may not be obvious. Fractures aligned parallel to wave propagation could change the response of Q_s/Q_p versus V_p/V_s ratios to water saturation from previously reported trends. Shear wave splitting due to the presence of aligned fractures results in two velocity ratios (V_p/V_{s1} and V_p/V_{s2}). The fluid independence of shear wave splitting for fractures aligned parallel to wave propagation direction means the difference between V_p/V_{s1} and V_p/V_{s2} is independent of water saturation. For fractures aligned at oblique angles, shear wave splitting can be sensitive to water saturation and consequently frequency-dependent, which can lead to fluid and frequency dependent difference between V_p/V_{s1} and V_p/V_{s2}. The effect of aligned fractures on V_p/V_s ratios not only depends on the fracture effects on both P- and S-wave velocities but also on the effects of water saturation distribution on the rock and fracture stiffness, and hence on the P- and S-wave velocities. As such, these effects can be frequency-dependent due to wave-induced fluid

flow. A simple modelling study combining a frequency-dependent fractured rock model and a frequency-dependent partial saturation model was used to gain valuable interpretations of our experimental observations and possible implications, which would be useful for field seismic data interpretation.

1. INTRODUCTION

Relating measured seismic properties (e.g. velocity and attenuation) to the physical properties of rocks (e.g. lithology, fluid content, fractures) is an important aspect of seismic exploration. Many existing relationships between seismic properties and physical properties of rocks have been established for non-fractured rocks; however, many reservoir formations contain fractures which are usually aligned. The effects of aligned fractures on these relationships are still not well explored. Elastic wave properties in rocks depend on the rock properties (e.g. porosity, pore/grain geometry, matrix mineral) and the pore fluid. The fact that the individual properties are sensitive to several parameters means observation of a single property alone may not be sufficient for characterizing rocks. However, since both P- and S-waves respond differently to changes in rock physical properties (e.g. saturation), S-waves have been suggested as a normalizing quantity with which to compare P-wave properties (e.g. Pickett 1963, Tatham and Stoffa 1976, Winkler and Nur 1982, Klimentos 1995).

The ratio of P- to S- velocity (V_p/V_s) has long been shown to be sensitive to lithology, saturation and porosity (Pickett 1963, Castagna, Batzle and Eastwood 1985) and has since been a commonly used tool in exploration seismology and formation evaluation. Similar relationships between attenuation and petrophysical properties of rocks have been sought with much less success and we are still far from inferring petrophysical properties from attenuation than from velocities (Dvorkin and Mavko 2006). However, the ratio of P- to S-wave attenuation (Q_s/Q_p) has been shown to be a good discriminator of partial gas/water saturation and to be more sensitive to the amount of water saturation over a wider range than the velocity ratio (Murphy 1982, Winkler and Nur 1982, Klimentos 1995). Consequently, Winkler and Nur (1982) suggested that combining both Q_s/Q_p and V_p/V_s could improve estimation of the degree of saturation. Velocity ratios have therefore been extensively applied to the interpretation of seismic data for petrophysical and fluid properties and attenuation ratios with more limited

applications have been used for fluid discrimination (Klimentos 1995, Sun *et al.* 2000, Koesoemadinata and McMechan 2001, Dvorkin and Mavko 2006). Studies combining both attenuation and velocity data for saturation estimation are limited and, furthermore, are constrained to approximately isotropic rocks. In particular, the effect of aligned fractures on these relationships is still poorly understood even though such conditions are common in the Earth's crust.

Rocks containing aligned fractures exhibit seismic anisotropy and shear wave splitting (SWS); hence, in anisotropic rocks, these ratios would not be unique and would depend on the direction and orientation of wave propagation. As such, for every direction, there would be two P- to S-wave ratios except in the direction of the symmetry axis where no SWS is expected. Therefore, the P- to S-wave ratios would depend on the effect of the rock-fluid properties and the fracture properties (e.g. SWS). The experimental results of Amalokwu *et al.* (2014) showed that the presence of fractures aligned in the direction of wave propagation not only results in attenuation anisotropy as expected but could also change the relationships that have been shown to be common in non-fractured rocks. Although the fluid and frequency dependence of SWS at oblique angles have been shown theoretically and observed experimentally (Chapman 2003, Qian *et al.* 2007, Tillotson *et al.* 2011), Amalokwu *et al.* (2015b) showed that partial liquid/gas saturation could also have this effect. Therefore, at oblique angles the difference between V_p/V_{s1} and V_p/V_{s2} could depend on the fluid, and hence on wave frequency. S1 and S2 represent the fast and slow shear waves polarised parallel and perpendicular to the fractures, respectively.

In this study, we present experimental results comparing the effects of water saturation (S_w) on Q_s/Q_p versus V_p/V_s ratios between a non-fractured rock and one containing fractures aligned parallel to direction of wave propagation. Although some of the data presented in this work has been presented in previous publications (Amalokwu *et al.* 2014, Amalokwu *et al.* 2015b), they are presented here for completeness. This paper adds the effects on velocity ratios, combining

both attenuation and velocity effects, and focuses on the implications of the results through qualitative interpretation with the help of some theoretical modelling. The results suggest that aligned fractures can change the Q_s/Q_p versus V_p/V_s ratios from the trends previously observed in the literature. We also study the effects of water saturation on V_p/V_s ratios in a rock containing fracture aligned at 45^o to wave propagation direction. Following Amalokwu *et al.* (2015a,b), we combine a model for partial saturation and the model of Chapman (2003) for saturated rocks containing aligned fractures both of which are frequency-dependent, to explain our experimental observations for the V_p/V_s ratios. As expected, V_p/V_{s2} ratio depends on the amount of SWS. Although we did not measure the V_p/V_s ratio for fractures aligned perpendicular to the direction of wave propagation in this study, the modelling study gives some interesting insights into what could be expected for this case, and is supported by previous experimental observations (Tillotson *et al.* 2014, Amalokwu *et al.* 2015a). This direction has the lowest V_p/V_s ratio for the dry case; however, the fluid acts to stiffen the fractures, hence stiffening the rock to compression, but saturation leads to a decrease in shear wave velocity due to the effect of bulk density. This in turn leads to a greater increase in V_p/V_s ratios from the dry state compared to the increase seen in other directions.

2. METHODS

2.1. Synthetic rock samples

A summary of the synthetic rock manufacturing process is presented here as the process is well documented by Tillotson *et al.* (2012). A non-fractured (blank) sample was made as a control sample along with a set of fractured samples. The samples were made from a mixture of sand, kaolinite, and aqueous sodium silicate gel. Fractures were created using a similar approach to (Rathore *et al.* 1995), by arranging a predetermined number of 2 mm diameter aluminium discs of 0.2 mm thickness on successive 4 mm layers of sand mixture. The rocks were baked and then cored at 45^o and parallel to wave propagation direction (90^o fractured sample). The rock

was cored parallel to the layers in the case of the blank sample. Figure 1 shows a schematic of the layer/fracture orientations within the rock samples. The aluminium discs were leached out with acid to leave penny-shaped voids in the silica-cemented sandstones. Image analysis of X-ray CT scans was used to obtain the fracture density, $\varepsilon_f = 0.0298 \pm 0.0077$ and an average fracture aspect ratio of 0.088 ± 0.001 (see Tillotson *et al.* 2012) for the sample containing vertically aligned fractures. The fracture density of the sample containing fractures aligned 45^o to wave propagation direction was not obtained using X-ray CT scans, however, both samples were made as part of the same batch and as such we will assume similar fracture properties (Amalokwu *et al.* 2015b). The porosity and Klinkenberg corrected permeability were measured using Helium porosimetry and Nitrogen permeametry respectively and are given in Table 1. Note the difference in permeability between the samples, attributed to differences in grain packing during rock manufacturing stage and the direction in which the rocks were cored as permeability was measured in the direction of the core axis.

2.2. SATURATION METHOD

The saturation methods used are detailed in an earlier paper (see supplementary information section of Amalokwu *et al.* 2014). Partial water saturation was achieved using a combination of two methods which aim to avoid/minimize heterogeneous saturation distribution. The samples were placed in an atmosphere of known and controlled relative humidity (RH) for about two weeks, until they had reached equilibrium. This method is known to give homogeneous S_w distributions for the lower S_w values (compared to imbibition and drainage); similar methods have been used elsewhere (Schmitt, Forsans and Santarelli 1994, Papamichos, Brignoli and Santarelli 1997, King, Marsden and Dennis 2000). The relative humidity was controlled using aqueous saturated salt solutions. Greenspan (1977) gave a range of salt solutions that would maintain a given RH at a particular temperature. The maximum S_w

achieved using this method was about 0.4 for the blank rock and the 90^{o} fractured sample, and 0.2 for the 45^{o} fractured rock.

To achieve intermediate S_w values, we used a modified air/water drainage technique. In order to minimise effects of heterogeneous saturation distribution caused by drainage (Cadoret, Marion and Zinszner 1995, Knight, Dvorkin and Nur 1998), the samples were wrapped in plastic ("cling") film after each drainage process. The wrapped samples were then placed in a desiccator containing the 98% RH solution, sealed (not vacuum sealed) and left for a minimum of 48 hours. The plastic film (and also the high RH atmosphere) prevented further air/water drainage, thus allowing capillary re-distribution over the length of time left to equilibrate ($\geq$ 48 hours). Although we took steps to minimize heterogeneous distribution saturation, the objective was to observe differences between the blank rock response and the fractured rocks. Full water saturation was achieved using the method described by McCann and Sothcott (1992).

2.3. ULTRASONIC EXPERIMENTS

Ultrasonic wave phase velocity and attenuation coefficient were measured at different air/water saturation (S_w) states to accuracies of ± 0.3% and ± 0.2 dB/cm respectively using the pulse reflection method (see Best, Sothcott and McCann 2007, Tillotson *et al.* 2012). P- and S-wave velocity measurements were made on all three samples. Shear-wave splitting was measured by rotating the piezoelectric shear-wave transducer (while the sample was under elevated pressure) and observing the maximum and minimum signal amplitudes corresponding to S1 and S2 waves, respectively (see Best *et al.* 2007, Tillotson *et al.* 2012). The equations of Dellinger and Vernik (1994) were used to ensure we were measuring a phase velocity for the 45^{o} sample (see Amalokwu *et al.* 2015b).

We did not measure attenuation for the 45^o sample because of difficulties in obtaining reliable attenuation measurements for this sample. Our pulse-echo method is sensitive to the presence of heterogeneities that are not sufficiently smaller than the ultrasonic wavelength. A typical P-wave trace from the 45^o sample (Figure 2) shows a multiple arrival which separates the reflection from the top of the rock from that from the base of the rock compared to the cleaner waveforms for the blank and 90^o rock samples shown by Amalokwu *et al.* (2014). There is no way to accurately take this into account in the calculation of the reflection coefficient that goes into the attenuation calculation (see Best, McCann and Sothcott 1994, Best *et al.* 2007). This and the fact that we do not have the full elastic tensor of the rock in order to calculate the anisotropic reflection coefficient makes it difficult to obtain reliable attenuation measurements from the 45^o sample. Therefore, attenuation was only calculated for the blank and 90^o fractured sample. It should be pointed out that the shear waveforms do not show this multiple arrival in the 45^o sample as shown by Amalokwu *et al.* (2015b), hence we show only a P-wave example.

A major issue with fractured rock experiments is scattering attenuation, which is undesirable as we are interested in intrinsic attenuation. Scattering attenuation becomes significant when the size of the heterogeneity becomes comparable to the elastic wavelength (Blair 1990, Liu *et al.* 2003). As pointed out by Amalokwu *et al.* (2014), we do not expect significant contributions from scattering attenuation for the P- and S1- waves in the 90^o sample as we measure Q_p^{-1}, Q_{s1}^{-1} parallel to the fractures (see Figure 1b). This is because amplitudes of the P- and S1-waves propagating parallel to the fractures depend mainly on the fracture aperture (thickness) and not the diameter of the fractures (Wei and Di 2008, de Figueiredo *et al.* 2013). In our ultrasonic pulse-echo experiments, the wavelength is approximately 5 mm and 3 mm for P- and S1-waves, respectively, and the ratio of wavelength to fracture aperture (0.2 mm) is ~ 25 and 16, respectively, suggesting that the presence of fractures should not contribute significantly to scattering attenuation for wave propagation parallel to wave propagation direction.

3. RESULTS

All results are presented at an effective pressure of 40 MPa (pore fluid pressure equal to atmospheric pressure) and a single frequency of 650 kHz obtained from Fourier analysis of broadband signals.

3.1. VELOCITY RATIOS

All three samples show fairly similar V_p/V_s trends. The blank rock sample has a dry value of ~ 1.58 (Figure 3) and shows an increase between $S_w \approx 0.03$ and $S_w \approx 0.09$ where it remains fairly constant up to $S_w \approx 0.4$, followed by a sharp increase at $S_w \approx 0.5$, increasing steadily to a maximum of $1.76 \pm 0.6\%$ at $S_w = 1.0$. The observed V_p/V_s ratios are in agreement with values reported for clean sandstones (Gregory 1976, Castagna *et al.* 1985, Brie *et al.* 1995).

In the 90° fractured sample (Figure 4a), both V_p/V_{s1} and V_p/V_{s2} show similar behaviour to the blank sample except for V_p/V_{s1} and V_p/V_{s2} between $S_w \approx 0.6 – 0.9$ being higher than the values for $S_w = 1.0$. The 90° fractured sample has dry V_p/V_{s1} and V_p/V_{s2} values of ~ 1.56 and 1.61 respectively. The slower S2 wave shows the presence of fractures can also cause an increase in measured V_p/V_s ratios. The difference between V_p/V_{s1} and V_p/V_{s2} remains fairly constant from dry to full water saturation.

In the 45° fractured sample (Figure 4b), although we do not see the same amount of increase at $S_w \approx 0.1$, the trend is similar to that observed for the blank and 90° samples. The 45° fractured sample has dry V_p/V_{s1} and V_p/V_{s2} values of ~ 1.56 and 1.59 respectively. The difference between V_p/V_{s1} and V_p/V_{s2} remains constant between dry and $S_w \approx 0.7$, after which the difference begins to decrease until full water saturation.

3.2. SHEAR WAVE SPLITTING

To understand the differences between the V_p/V_{s1} and V_p/V_{s2} it is useful to study shear wave splitting. Shear-wave splitting is expressed as SWS (%) = 100 × (S1 − S2)/S1, where S1 and S2 are the parallel and perpendicular shear-wave velocities relative to the fracture direction, respectively. Figure 5 shows the SWS in the blank sample; both V_{s1} and V_{s2} have similar values for all S_w showing that SWS induced by layering is negligibly small (~ 0.4 ± 0.6%) and stays fairly constant for all S_w values.

The 90^o fractured sample shows significant SWS (Figure 6a) as expected as a result of the fractures. Similar to the blank sample, the SWS stays fairly constant for all S_w values. Similar observations of the fluid independence in this direction has been made (e.g. Rathore *et al.* 1995, Tillotson *et al.* 2012) and predicted by theory (e.g. Hudson 1981, Xu 1998, Giraud *et al.* 2007).

The 45^o fractured sample also shows significant SWS (Figure 6b) compared to the blank sample but less than that observed in the 90^o fractured sample S_w. Shear-wave splitting begins at ~ 2 ± 0.6% at S_w = 0 (dry), remaining fairly constant until $S_w \approx 0.7$, then followed by a steady decrease between $S_w \approx 0.8 - 1.0$. This shows that SWS due to fractures aligned at oblique angles to wave propagation direction can be sensitive to water saturation at higher S_w values, something not observed in either the blank or 90^o fractured sample

3.3. Q_S/Q_P RATIOS

The ratio of Q_p^{-1} to Q_s^{-1} has been presented by Amalokwu *et al.* (2014) but we present it here again for completeness as we will be comparing Q_s/Q_p versus V_p/V_s ratios in the analysis to come. We only measured attenuation for the blank and 90^o samples. For approximately isotropic rocks, the Q_s/Q_p ratio is greater than unity for $S_w < 0.9$ and less than unity at higher saturations (e.g. Murphy 1982), which is also in good agreement with our observations for the

blank rock (Figure 7a). Although there is negligible SWS induced by layering, Q_{s1}^{-1} and Q_{s2}^{-1} are similar so we only plot Q_{s1}/Q_p (see Amalokwu *et al.* 2014).

However, our results show markedly different behaviour in the fractured rock. For the 90° fractured sample, Q_s/Q_p is only significantly greater than 1 at intermediate saturations of about $S_w = 0.45$ for fast S-waves only (S1) (Figure 7b). Otherwise, Q_s/Q_p is about unity (± 0.2) except at low saturations ($S_w < 0.1$) and high saturations ($S_w > 0.8$) for both fast (S1) and slow (S2) shear waves for which Q_s/Q_p is less than 1.

These observations show that the presence of aligned fractures can significantly change the Q_s/Q_p relationships previously established for approximately isotropic rocks.

3.4. V_P/V_S VERSUS Q_S/Q_P

The ratio of Q_p^{-1} to Q_s^{-1} when combined with the ratio of P- to S-wave velocity could give a more precise estimate of the degree of saturation (Winkler and Nur 1982). In the blank rock (Figure 8a), the Q_s/Q_p ratio is greater than unity for $S_w < 0.9$ and less than unity at higher saturations (e.g. Murphy 1982, Winkler and Nur 1982), with the reference line of $Q_s/Q_p = 1$ clearly separating partial saturation from full water saturation. For the V_p/V_s ratios, dispersion is evident from the gradual increase from dry to water saturation. This dispersion results in a spreading out of V_p/V_s values with the general trend being higher saturation values plotting towards the right (higher V_p/V_s) ratios. This is in contrast to the low frequency observations and low frequency theoretical predictions (Gassmann-Wood) where the V_p/V_s values for both dry and partially saturated states essentially have the same values and as such would cluster together (e.g. Murphy 1982, Winkler and Nur 1982). In practice, it has been shown that the low frequency observations may not always be consistent with sonic well log observations due to dispersion (e.g. Brie *et al.* 1995, Caspari, Müller and Gurevich 2011). In the presence of this velocity (and hence V_p/V_s) dispersion due to wave-induced fluid flow, the reference line of

$Q_s/Q_p = 1$ still clearly separates partial saturation from full water saturation. As such, combining both Q_s/Q_p and V_p/V_s ratios could help improve gas discrimination by reducing the possible ambiguity associated with velocity dispersion, which could cause higher V_p/V_s ratios for partially saturated rocks (for example, at higher frequencies of sonic well logs).

One mechanism that has been suggested to explain the Q_s/Q_p behaviour is viscous loss from inter-crack fluid flow; bulk compression from P-waves generates more inter-crack flow than S-waves in partially saturated rocks while the reverse is the case in 100% water saturated rocks (Winkler and Nur 1979, Winkler and Nur 1982). There is considerable literature addressing water saturation effects on attenuation and velocities (e.g. Winkler and Nur 1982, Murphy 1984, Gist 1994, Müller, Gurevich and Lebedev 2010). Here we will focus on the differences between the blank rock response and those from the samples containing aligned fractures.

The 90^o fractured rock (Figure 8b) shows a similar behaviour to the blank rock in terms of the V_p/V_s trend where the higher S_w values plot towards higher values of V_p/V_s ratios. There is significant shear wave splitting as expected, resulting in two V_p/V_s ratios. Therefore, the V_p/V_s ratio is not unique and depending on direction of wave propagation and on S-wave polarization, V_p/V_s ratio would be different as expected for an anisotropic medium.

The first thing to note about the attenuation ratios in the fractured rock is the reduction in magnitude of the ratios (the plot is pushed down). As a result, the attenuation ratios are not clearly separated by the reference value of $Q_s/Q_p = 1$ (compared to the blank sample) as partial saturation values fall below the reference line, with the Q_p/Q_{s2} ratios falling even lower. For wave propagation parallel to the fractures, the three waves (P, S1, S2) respond differently to the extra weakness introduced by the presence of the fractures as they propagate in different planes relative to the fractures. P-wave attenuation is not significantly increased by the presence of fractures as long as the fracture aperture is much less than the wavelength (e.g.,

Wei and Di 2008); however, the presence of fractures appears to increase both Q_{s1}^{-1} and Q_{s2}^{-1} (the effect being greater on Q_{s2}^{-1}). This produces a striking difference in the Q_s/Q_p versus saturation relationship from that seen in the blank sample (see Amalokwu *et al.* 2014). This could lead to interpretation errors when using Q_s/Q_p as a diagnostic tool for fluid saturation.

4. DISCUSSION

Although all three samples were made from a single batch of constituents, there are still small microstructural differences associated with the manufacturing process and as such they cannot all be considered to have the same background material. Also, the fact that the samples were packed in different moulds mean that there are some little differences in fracture parameters between both fractured samples. This prevents interpretations and comparisons of absolute values; however, we can interpret differences in trends observed.

Seismic attenuation and velocity dispersion are now widely accepted to be caused by wave-induced fluid flow mechanisms (Mavko and Nur 1979, Winkler and Nur 1979, Murphy 1982, Winkler and Nur 1982, Murphy, Winkler and Kleinberg 1986, Müller *et al.* 2010). Different viscous loss mechanisms have been proposed to quantify attenuation and velocity dispersion observed in both field and experimental data; Müller *et al.* (2010) give a detailed review. However, several challenges still remain that make currently existing models unsatisfactory such as the necessary reliance on parameters that are not readily available or are unknown (e.g. squirt-flow radius, relaxation timescales and other microstructural details) (Winkler and Nur 1982, Dvorkin and Mavko 2006), the lack of a satisfactory unified framework for different viscous mechanisms which are possibly competing or co-existing (Winkler and Nur 1982, Gist 1994, Wu *et al.* 2014).

The ambiguities associated with the rock manufacturing process, and the fact that there are still no suitable frequency-dependent theoretical models for elastic wave velocities in partially

saturated fractured rocks, mean we will seek to understand the results and their implications through a more qualitative interpretation with the help of existing theoretical mechanisms and models. In the model of White (1975), shear waves are unaffected by saturation and as such, no shear wave dispersion or attenuation is predicted. Also, the model of Chapman (2003) only considers fluid effects and predicts no dispersion in bulk or shear for wave propagation at 90^o to the fracture normal. Therefore, we cannot model the difference in observed experimental attenuation trends between the blank and 90^o fractured rock samples.

We will instead focus on discussing possible mechanisms causing the observed effects of aligned fractures on the observed V_p/V_s trends by using a simple modelling approach. We would like to stress that the mechanisms suggested here are not the only mechanisms (or combination of mechanisms) that can explain the data and is just an example of how a combination of mechanisms can produce these effects.

4.1. Modelling of V_P/V_S AND SWS

Our results show that as expected, high V_p/V_s ratios can be observed for wave propagation in rocks containing aligned fractures depending on the shear wave polarizations ($V_p/V_{s2} > V_p/V_{s1}$). These differences in V_p/V_s ratios would depend on SWS which in turn is related to the fracture density. Consequently, understanding the effects of aligned fractures on V_p/V_s ratios requires an understanding of the SWS behaviour as well.

Shear wave splitting for waves propagating parallel to the fractures has been shown to be independent of saturating fluid (e.g., Tillotson *et al.* 2012), in agreement with our observations (Figure 6a), however, at oblique angles fluid compressibility can affect SWS. Amalokwu *et al.* (2015b) showed that water saturation can affect SWS in rocks containing fractures aligned at oblique angles and that this fluid effect can be frequency-dependent. This fluid-sensitivity is due to the fact that the S2 wave is sensitive to the fluid compressibility when the fractures are

aligned at oblique angles to the direction of wave propagation. The modelled effect of partial gas saturation on SWS presented by Amalokwu *et al.* (2015b) was not very significant, however, it was implied that the effect could increase if additional viscous mechanisms were considered. Amalokwu *et al.* (2015a) showed that the effects of water saturation on P-wave anisotropy can be significant depending on the mixing of the liquid and gas (water and air) at the crack/pore scale. Considering this crack/pore-scale mixing, we will repeat the modelling study of (Amalokwu *et al.* 2015b) to explain our experimental observations.

4.1.1. Modelling approach

The modelling approach combines the fractured rock model of Chapman (2003) and the partial saturation model of White (1975). The stiffness tensor, C_{ijkl}, given by Chapman (2003) relating the contributions from the isotropic elastic tensor (C^0, with Lamé parameters, λ and μ), C^1 (pores), C^2 (microcracks) and C^3 (fractures) scaled by the porosity (Φ_p), microcrack density (ε_c) and fracture density (ε_f) is of the form:

$$C_{ijkl} = C^o_{ijkl} - \Phi_p C^1_{ijkl} - \varepsilon_c C^2_{ijlk} - \varepsilon_f C^3_{ijkl} \quad (1)$$

This model is not designed for partial saturation, so in the elastic tensors, we replace all terms apart from the fracture correction, with the Lamé parameters λ^o and μ^o obtained from the model of White (1975) for each water saturation value. The Lamé parameters λ^o and μ^o from White's model already contain porosity effects, and as shown by Chapman *et al.* (2003), ε_c can be set to zero in high porosity rocks which would make the contribution from C^2 zero. We now have an equation of the form:

$$C_{ijkl} = C^{iso}_{ijkl}(\lambda^o, \mu^o) - \varepsilon_f C^3_{ijkl}; \quad (2)$$

where the term C^{iso}_{ijkl} is obtained from the Lamé parameters λ^o and μ^o calculated using the model of White (1975) (see Mavko, Mukerji and Dvorkin 2009, p. 327), after which the fracture

correction C^3 (see Chapman *et al.* 2003 p. 200) is applied. It should be pointed out here that the Lamé parameter, μ^o is the rock shear modulus which is unaffected by saturation in White's model. The frequency-dependent partial ("patchy" in the case of White's model) effect in the background rock comes in through White's model because the model of Chapman *et al.* (2003) was not developed for multiphase saturation. We are not suggesting that the dispersion in our experiments is restricted to patchy saturation. The idea is to achieve frequency-dependent bulk moduli due to the presence of partial saturation. White's model in the above equation could be replaced with any other partial saturation model. For example we could use Gassmann's theory with an effective fluid modulus from Brie's equation and still obtain a decent fit.

Modelling parameters are the same as those used by Amalokwu *et al.* (2015b) and also given in Table 2. In order to adapt the model of Chapman (2003) for partial multiphase saturation modelling, we require an effective modulus as input for the fluid bulk modulus in the fracture model. Amalokwu *et al.* (2015b) considered this fluid modulus to be the Reuss average of air and water which corresponds to a uniform fluid mix so the wave-induced pore pressures have enough time to equilibrate during a seismic period (Mavko and Mukerji 1998). The result obtained in this case predicted no stiffening effects due to a reduction in fracture compliance as a result of partial saturation as there is always time for any wave induced pressures to equilibrate. Therefore the effective fluid modulus within the fractures would be that of the fluid with the lower bulk modulus (air in this case) except at about $S_w > 0.95$. It might not always be the case that the fluids within the fractures are mixed uniformly; for example, in a partially saturated fracture, the wetting fluid phase (e.g. water) could preferentially adhere to the rock surface, leaving patches of air/water within the fractures since it is not fully saturated. In this case, the Reuss averaged bulk modulus might not be sufficient to describe the effective fluid bulk modulus effect on the fractures.

To explore this scenario, following Amalokwu *et al.* (2015a) we will assume that air and water are not uniformly mixed within the fractures and as such take a non-Reuss averaged fluid modulus as the effective fluid modulus for input into the model of Chapman (2003). This can be viewed for example as some sort of patchy saturation distribution (which we do not make explicit) within the fractures. To achieve this, for simplicity, we will assume the stiffening effect resulting from the saturation distribution within the fractures is the same as that from White's effect in the rock matrix instead of using fluid mixing equations (e.g. Brie *et al.* 1995) or explicitly calculating a dynamic fluid modulus (e.g. Yao *et al.* 2015). As pointed out by Amalokwu *et al.* (2015a), this is probably not the case in reality but taking this approach would give us a reference frequency for the fluid bulk modulus effect in the background isotropic rock model and the fractured rock model. We will refer to this approach as **'assumption 1'**. This assumption is restrictive as we cannot fit the V_p/V_s trend in the rocks and the SWS at the same time using this approach. However this is sufficient as at this point we are more concerned with the effect of saturation on SWS and how this in turn affects the behaviour of the V_p/V_s ratios relative to direction of propagation. We will later show that relaxing this assumption, we can get a better fit to the V_p/V_s versus S_w behaviour as well as a good fit to the SWS by relaxing 'assumption 1'. This second modelling approach will be denoted as **'assumption 2'**. We calculate the frequency-dependent saturated bulk modulus using White's model using a patch size of 0.5 mm chosen (as a fitting parameter) to fit the water saturation where the SWS in the experimental data begins to decline. This modulus should be reproducible with Gassmann's equation using a suitable "effective" fluid modulus, which we solve for. This is done by taking the real part of the bulk modulus obtained from White's model at each frequency as the saturated rock bulk modulus and then solve Gassmann's equation for the fluid bulk modulus (see Amalokwu *et al.* 2015a).

4.1.2. Modelling results - Assumption 1

Figure 9a shows the frequency-dependent bulk modulus versus S_w obtained from White's model for the isotropic background rock and Figure 9b shows the corresponding effective fluid modulus calculated from Gassmann's formula as described above. Figure 10a shows the modelling of the experimental results of SWS for the 90° sample while Figure 10b shows the best fitting model for the 45° sample when there is no dispersion and when there is dispersion from the fractured sample. For waves propagating parallel to the fractures, no fluid dependence is seen, in general agreement with our observations and previous studies. At 45° to the fracture normal, a fluid dependence (and hence frequency-dependence) of SWS can be seen. Amalokwu *et al.* (2015a) showed that this approach better explained the water saturation effects on P-wave anisotropy. This same approach appears to also better explain our experimental observations of water saturation effects on SWS when fractures are aligned at oblique angles and as such could give valuable insight into the trends observed. The goal here is to illustrate the potential effect of this additional dispersion from the fractures due to the presence of partial saturation although the specific mechanisms used to achieve this may not represent the actual mechanisms responsible for our experimental observations.

The 90° fit was achieved by taking the fracture density of 0.029 stated above, while the best fit for the 45° sample was achieved by also taking a fracture density of 0.023, within the uncertainty range given above, and using microcrack relaxation timescale $\tau_m = 1.6 \times 10^{-8}$ s. This relaxation time was chosen to fit the SWS at $S_w = 1$, and is similar to the value given by Tillotson *et al.* (2014), who estimated a value of 2.4×10^{-8} s for comparable synthetic sandstones. Both fracture aspect ratios are taken as 0.088 obtained from CT images of the 90° sample. Using this resulting model for partial saturation effects in fractured rocks, we can better understand the effects of saturation on the behaviour of the V_p/V_s ratios in rocks containing aligned fractures. Plotting V_p/V_{s1} and V_p/V_{s2} parallel to the fractures (Figure 11a), we can see that apart from the SWS, this would show a similar behaviour to the blank rock behaviour as

the shear waves are not dependent on saturation. Consequently, the difference between V_p/V_{s1} and V_p/V_{s2} would remain the same for a given fracture density, independent of water saturation, in general agreement with our observations. Depending on the fracture properties, even higher V_p/V_{s2} ratios could be measured and if anisotropy is not taken into account could be misinterpreted, for example, as a different lithology. For oblique angles (e.g. 45^o to wave propagation direction) (Figure 11b), the general V_p/V_{s1} and V_p/V_{s2} trend would be similar to that of the blank and the 90^o fractured sample; however, both P- and S-2 waves would be sensitive to water saturation and hence frequency-dependent. Therefore the difference between V_p/V_{s1} and V_p/V_{s2} would be saturation dependent as SWS would be saturation dependent (Figure 11b). A decrease in the difference between V_p/V_{s1} and V_p/V_{s2} can be seen at higher values of S_w, which is in agreement with our experimental observations.

Although we do not have measurements for waves propagating perpendicular to the fractures, this modelling exercise could give some insight into the effect of water saturation on the V_p/V_s ratio in this direction. There is no shear wave splitting as expected in this direction and the general trend is similar to the other directions, so only one V_p/V_s ratio is expected in this direction. The interesting thing to note is that in this direction, the fractures are a lot more compliant to compression, as such the P-wave velocity is much more affected by the fractures compared to the shear wave velocity. This would give a lower dry (or air) V_p/V_s ratio in this direction because the fracture filling fluid is very compressible. However, as S_w increases and begins to stiffen the fractures, the rock P-wave modulus increases significantly compared to its dry value while the shear stiffness is unaffected; hence the V_p/V_s ratio increases significantly at high to full water saturation (depending on frequency effects). This direction would be expected to show the highest increase in V_p/V_s ratio from dry to full water saturation (Figure 12). This suggests that although shear wave splitting is not observed in this direction, the presence of saturated fractures could lead to high V_p/V_s ratios being measured in this direction.

This was shown by the modelling study of Wang *et al.* (2012) and is supported by the experimental observations of Tillotson *et al.* (2014) and Amalokwu *et al.* (2015a). In practice, this scenario is possible in cross-well surveys where there are vertically aligned fractures; for example, an initially fully liquid saturated (e.g. oil) reservoir would show a significant decrease in V_p/V_s ratio compared to a non-fractured rock as the oil is produced without liquid replacement and gas comes out of solution as a result of the drop in reservoir pressure.

4.1.3. Modelling results – Assumption 2

To obtain a better fit for both the S_w dependence of V_p/V_s trend and SWS trend, we have to relax the assumption that the stiffening effect in both the background matrix and the fractures is the same. This assumption was made for simplicity and reduces the number of free variables. Without this requirement, a different effective fluid modulus would have to be fitted to the fractured rock model as opposed to the consistency between both models. Another implication of the way the modelling was implemented is the implicit assumption the S_w in the background and the fractures are the same at any point in time which in reality might not be the case. Larger fractures might drain quicker than smaller pores and might be almost empty by the time the pores in the background rock still contained high amounts of water saturation. This situation is not considered here but could potentially be explored with the present implementation setup which allows the fluid effects to be accounted for separately in both the fractures and background matrix. In order to achieve better fit for the V_p/V_s trend and a decent fit for the SWS trend using the same modelling implementation, we take the stiffening effects from saturation to be different in the background matrix and the fractures. To do this we take the patch size in White's model to be 2 mm which also gives a good qualitative fit to the attenuation data (see Amalokwu *et al.* 2014), but in the fractured rock model we use a fluid modulus from the mixing law of Brie *et al.* (1995). The exponent in the equation of Brie *et al.* (1995) is chosen to fit where the stiffening effect from the fracture begins ($S_w \approx 0.7$) and an exponent of 6 was

chosen (values between 5-8 give good fits as well). All other parameters used are the same as those used in 'assumption 1'. Figure 13 shows the model fit for the V_p/V_s ratios versus S_w for the blank (Figure 13a) and 90^o fractured sample (Figure 13b). Figure 14a shows the model fit for the V_p/V_s ratios versus S_w for the 45^o fractured sample, while Figure 14b shows its corresponding SWS versus S_w fit to the model. It can be seen that a good fit to the model can be obtained for both the V_p/V_s and the SWS. This suggests that in terms of partial saturation effects on SWS, the contribution from the effects in the background rock is subtle and the additional dispersion from the fractures is the more important contribution (Figures 10b and 14b). So it appears the stiffening effect from the fractures occur at higher water saturation in this present experiment, which would make sense as we would expect the fractures to preferentially drain relative to the background rock matrix.

Plotting V_p/V_{s1} and V_p/V_{s2} (Figure 15) provides us with another way of visualizing the effects of aligned fractures on V_p/V_s ratios and of comparing our experimental trends to our modelling results (from Figures 13 and 14). We can see the relationship between V_p/V_{s1} and V_p/V_{s2} gives a straight line and the experimental trend follows the trend predicted by the model even in the presence of additional dispersion (and other ambiguities in the data) not considered in the modelling, which also leads to an under-prediction of the upper limit of the V_p/V_s ratios.

5. CONCLUSIONS

We have presented experimental observations of possible effects of aligned fractures on the response of V_p/V_s and Q_s/Q_p ratios to water saturation compared to observations in non-fractured rocks. We used synthetic porous sandstones that provide realistic analogues to naturally occurring sandstones. The results for the blank sample support previous suggestions that combining both V_p/V_s and Q_s/Q_p ratios could help improve partial/liquid gas saturation

discrimination. However, in the sample with fractures aligned parallel to wave propagation direction, although the trend and values of the V_p/V_s ratios are similar to those in the blank sample, the Q_s/Q_p ratios are reduced in magnitude and the separation between partial saturation and full saturation is not as clear as it is for the blank sample.

Partial-gas saturation in rocks could lead to frequency-dependent effects on the V_p/V_s ratios, and in rocks containing aligned fractures, this could lead to frequency-dependent anisotropic effects that could be amplified depending on the crack-scale effect of S_w on the fracture stiffness. Parallel to wave propagation direction, theory predicts shear wave splitting is not sensitive to saturation hence the difference between both V_p/V_{s1} and V_p/V_{s2} remains the same for all $S_{W;}$ this is in general agreement with our experimental observations. At 45^o degrees to wave propagation direction, both V_p and V_{s2} are sensitive to S_w and as such SWS and the difference between both V_p/V_{s1} and V_p/V_{s2} would depend on S_w (and frequency). The simple modelling study and previous results show that rocks with fractures aligned perpendicular to wave propagation direction would show the highest increase from dry to full water saturation. The modelling also showed that a Reuss averaged fluid modulus for the fractured rock model underestimates the effect of S_w on the dispersion observed at higher S_w values and as such provided a poor fit to the trends observed in the 45^o sample. However, an alternative fluid modulus average gives better agreement with the magnitude of dispersion observed which has a physical interpretation in terms of non-equal fluid pressures. These results could have important implications for seismic characterisation of fractured reservoirs. Further experimental and theoretical studies are needed for better understanding of these effects.

ACKNOWLEDGEMENTS

The authors wish to thank the United Kingdom Natural Environment Research Council and the sponsors of the Edinburgh Anisotropy Project for supporting this work which forms part of the PhD studies of Kelvin Amalokwu under a NERC-BGS PhD studentship. We would also like to thank Jeremy Sothcott for his help with the experimental design and setup. The authors wish to thank the associate editor Tobias Müller and three anonymous reviewers for their constructive reviews which helped improve the manuscript.

REFERENCES

Amalokwu K., Best A.I., Sothcott J., Chapman M., Minshull T. and Li X.-Y. 2014. Water saturation effects on elastic wave attenuation in porous rocks with aligned fractures. *Geophysical Journal International* **197**, 943-947.

Amalokwu K., Chapman M., Best A.I., Minshull T.A. and Li X.-Y. 2015a. Water saturation effects on P-wave anisotropy in synthetic sandstone with aligned fractures. *Geophysical Journal International* **202**, 1088-1095.

Amalokwu K., Chapman M., Best A.I., Sothcott J., Minshull T.A. and Li X.-Y. 2015b. Experimental observation of water saturation effects on shear wave splitting in synthetic rock with fractures aligned at oblique angles. *Geophysical Journal International* **200**, 17-24.

Best A.I., McCann C. and Sothcott J. 1994. The relationships between the velocities, attenuations and petrophysical properties of reservoir sedimentary rocks1. *Geophysical Prospecting* **42**, 151-178.

Best A.I., Sothcott J. and McCann C. 2007. A laboratory study of seismic velocity and attenuation anisotropy in near-surface sedimentary rocks. *Geophysical Prospecting* **55**, 609-625.

Blair D.P. 1990. A direct comparison between vibrational resonance and pulse transmission data for assessment of seismic attenuation in rock. *Geophysics* **55**, 51-60.

Brie A., Pampuri F., Marsala A. and Meazza O. 1995. Shear sonic interpretation in gas-bearing sands. Conference Shear sonic interpretation in gas-bearing sands.

Cadoret T., Marion D. and Zinszner B. 1995. Influence of frequency and fluid distribution on elastic wave velocities in partially saturated limestones. *Journal of Geophysical Research: Solid Earth* **100**, 9789-9803.

Caspari E., Müller T. and Gurevich B. 2011. Time-lapse sonic logs reveal patchy CO2 saturation in-situ. *Geophysical Research Letters* **38**.

Castagna J.P., Batzle M.L. and Eastwood R.L. 1985. Relationships between compressional-wave and shear-wave velocities in clastic silicate rocks. *Geophysics* **50**, 571-581.

Chapman M. 2003. Frequency-dependent anisotropy due to meso-scale fractures in the presence of equant porosity. *Geophysical Prospecting* **51**, 369-379.

Chapman M., Maultzsch S., Liu E. and Li X.-Y. 2003. The effect of fluid saturation in an anisotropic multi-scale equant porosity model. *Journal of Applied Geophysics* **54**, 191-202.

de Figueiredo J.J.S., Schleicher J., Stewart R.R., Dayur N., Omoboya B., Wiley R. and William A. 2013. Shear wave anisotropy from aligned inclusions: ultrasonic frequency dependence of velocity and attenuation. *Geophysical Journal International*.

Dellinger J. and Vernik L. 1994. Do traveltimes in pulse-transmission experiments yield anisotropic group or phase velocities? *Geophysics* **59**, 1774-1779.

Dvorkin J.P. and Mavko G. 2006. Modeling attenuation in reservoir and nonreservoir rock. *The Leading Edge* **25**, 194-197.

Giraud A., Huynh Q.V., Hoxha D. and Kondo D. 2007. Application of results on Eshelby tensor to the determination of effective poroelastic properties of anisotropic rocks-like composites. *International Journal of Solids and Structures* **44**, 3756-3772.

Gist G.A. 1994. Interpreting laboratory velocity measurements in partially gas-saturated rocks. *Geophysics* **59**, 1100-1109.

Greenspan L. 1977. Humidity Fixed Points of Binary Saturated Aqueous Solutions. *J. Res. Nat. Bur. Stand. (U.S.) - A (Phys. And Chem.)* **81A**, 89-96.

Gregory A. 1976. FLUID SATURATION EFFECTS ON DYNAMIC ELASTIC PROPERTIES OF SEDIMENTARY ROCKS. *Geophysics* **41**, 895-921.

Hudson J.A. 1981. Wave speeds and attenuation of elastic waves in material containing cracks. *Geophysical Journal of the Royal Astronomical Society* **64**, 133-150.

King M.S., Marsden J.R. and Dennis J.W. 2000. Biot dispersion for P- and S-wave velocities in partially and fully saturated sandstones. *Geophysical Prospecting* **48**, 1075-1089.

Klimentos T. 1995. Attenuation of P- and S-waves as a method of distinguishing gas and condensate from oil and water. *Geophysics* **60**, 447-458.

Knight R., Dvorkin J. and Nur A. 1998. Acoustic signatures of partial saturation. *Geophysics* **63**, 132-138.

Koesoemadinata A. and McMechan G. 2001. Empirical estimation of viscoelastic seismic parameters from petrophysical properties of sandstone. *Geophysics* **66**, 1457-1470.

Liu E., Queen J.H., Li X.Y., Chapman M., Maultzsch S., Lynn H.B. and Chesnokov E.M. 2003. Observation and analysis of frequency-dependent anisotropy from a multicomponent VSP at Bluebell-Altamont field, Utah. *Journal of Applied Geophysics* **54**, 319-333.

Mavko G. and Mukerji T. 1998. Bounds on low-frequency seismic velocities in partially saturated rocks. *Geophysics* **63**, 918-924.

Mavko G., Mukerji T. and Dvorkin J. 2009. *The Rock Physics Handbook.* Cambridge University Press.

Mavko G.M. and Nur A. 1979. Wave attenuation in partially saturated rocks. *Geophysics* **44**.

McCann C. and Sothcott J. 1992. Laboratory measurements of the seismic properties of sedimentary rocks. *Geological Society, London, Special Publications* **65**, 285-297.

Müller T., Gurevich B. and Lebedev M. 2010. Seismic wave attenuation and dispersion resulting from wave-induced flow in porous rocks — A review. *Geophysics* **75**, 75A147-75A164.

Murphy W., Winkler K. and Kleinberg R. 1986. Acoustic relaxation in sedimentary rocks: Dependence on grain contacts and fluid saturation. *Geophysics* **51**, 757-766.

Murphy W.F. 1982. Effects of partial water saturation on attenuation in Massillon sandstone and Vycor porous glass. *J. Acoust Soc. Am.* **71**, 1458–1468.

Murphy W.F. 1984. Acoustic measures of partial gas saturation in tight sandstones. *Journal of Geophysical Research: Solid Earth* **89**, 11549-11559.

Papamichos E., Brignoli M. and Santarelli F.J. 1997. An experimental and theoretical study of a partially saturated collapsible rock. *Mechanics of Cohesive-frictional Materials* **2**, 251-278.

Pickett G. 1963. Acoustic character logs and their applications in formation evaluation. *Journal of Petroleum Technology* **15**, 659-667.

Qian Z., Chapman M., Li X., Dai H., Liu E., Zhang Y. and Wang Y. 2007. Use of multicomponent seismic data for oil-water discrimination in fractured reservoirs. *The Leading Edge* **26**, 1176-1184.

Rathore J.S., Fjaer E., Holt R.M. and Renlie L. 1995. P- and S-wave anisotropy of a synthetic sandstone with controlled crack geometryl1. *Geophysical Prospecting* **43**, 711-728.

Schmitt L., Forsans T. and Santarelli F.J. 1994. Shale testing and capillary phenomena. *Int. J. Rock Mech. Min. Sci. & Geomech. Abstr.* **31**, 411 – 427.

Sun X., Tang X., Cheng C.H. and Frazer L.N. 2000. P- and S-wave attenuation logs from monopole sonic data. *Geophysics* **65**, 755-765.

Tatham R.H. and Stoffa P.L. 1976. Vp/Vs—A POTENTIAL HYDROCARBON INDICATOR. *Geophysics* **41**, 837-849.

Tillotson P., Chapman M., Best A.I., Sothcott J., McCann C., Shangxu W. and Li X.-Y. 2011. Observations of fluid-dependent shear-wave splitting in synthetic porous rocks with aligned penny-shaped fractures‡. *Geophysical Prospecting* **59**, 111-119.

Tillotson P., Chapman M., Sothcott J., Best A.I. and Li X.-Y. 2014. Pore fluid viscosity effects on P- and S-wave anisotropy in synthetic silica-cemented sandstone with aligned fractures. *Geophysical Prospecting* **62**, 1238-1252.

Tillotson P., Sothcott J., Best A.I., Chapman M. and Li X.-Y. 2012. Experimental verification of the fracture density and shear-wave splitting relationship using synthetic silica cemented sandstones with a controlled fracture geometry. *Geophysical Prospecting* **60**, 516-525.

Wang X.Q., Schubnel A., Fortin J., David E.C., Guéguen Y. and Ge H.K. 2012. High Vp/Vs ratio: Saturated cracks or anisotropy effects? *Geophysical Research Letters* **39**, L11307.

Wei J. and Di B. 2008. A physical model study of effect of fracture aperture on seismic wave. *Science in China Series D: Earth Sciences* **51**, 233-240.

White J.E. 1975. Computed seismic speeds and attenuation in rocks with partial gas saturation. *Geophysics* **40**, 224-232.

Winkler K. and Nur A. 1979. Pore fluids and seismic attenuation in rocks. *Geophysical Research Letters* **6**, 1-4.

Winkler K. and Nur A. 1982. Seismic attenuation: Effects of pore fluids and frictional-sliding. *Geophysics* **47**, 1-15.

Wu X., Chapman M., Li X.-Y. and Boston P. 2014. Quantitative gas saturation estimation by frequency-dependent amplitude-versus-offset analysis. *Geophysical Prospecting* **62**, 1224-1237.

Xu S. 1998. Modelling the effect of fluid communication on velocities in anisotropic porous rocks. *International Journal of Solids and Structures* **35**, 4685-4707.

Yao Q., Han D.-h., Yan F. and Zhao L. 2015. Modeling attenuation and dispersion in porous heterogeneous rocks with dynamic fluid modulus. *Geophysics* **80**, D183-D194.

TABLES

Petrophysical parameters	**Values**
Blank sample	
Porosity, φ_p	30.43%
Permeability, κ	40.7 mDarcy
90º Fractured sample	
Porosity, φ_p	31.68%
Permeability, κ	18.1 mDarcy
45º Fractured sample	
Porosity, φ_p	31.80%
Permeability, κ	2.66 mDarcy

Table 1. Petrophysical properties of synthetic sandstones.

Grain	
Bulk modulus	38 GPa
Shear modulus	44 GPa
Density	2590 Kg/m^3
Grain size	120 μm
Matrix	
Bulk modulus	10.27 GPa
Shear modulus	8.9 GPa
Density	1828 Kg/m^3
Porosity	30.43%
Permeability	40.7 mD
Gas (Air)	
Bulk modulus	0.0001GPa
Density	1.2 Kg/m^3
Viscosity	0.00002 Pa s
Water	
Bulk modulus	2.25 GPa
Density	1000 Kg/m^3
Viscosity	0.001 Pa s
Fracture properties	
Fracture density	0.0298 ± 0.0077
Average aspect ratio	0.088 ± 0.001

Table 2. Modelling parameters.

FIGURE CAPTIONS

Figure 1. Schematic showing the orientation of a) layering in the blank rock, fracture planes for the b) 90^o degree fractured sample and c) the 45^o degree fractured sample, relative to the direction of wave propagation.

Figure 2. Typical P-waveform for the 45^o sample showing reflections from (a) the top of the rock (window A) (b) the base of the rock (window B), clearly separated by reflections of significant amplitude from within the rock sample.

Figure 3. V_P/V_s versus S_w ratios for the blank rock (both fast S1 and slow S2 wave results are shown).

Figure 4. V_P/V_s versus S_w ratios for a) the 90^o fractured rock b) the 45^o fractured rock. Both fast S1 and slow S2 wave results are shown.

Figure 5. SWS versus S_w for the blank rock. Vertical error bar included.

Figure 6. SWS versus S_w for a) the 90^o fractured rock b) the 45^o fractured rock. Vertical error bar included.

Figure 7. Q_s/Q_p versus S_w for a) the blank rock b) the 90^o fractured rock.

Figure 8. Q_s/Q_p versus V_p/V_s ratios at different saturation values for a) the blank rock b) the 90^o fractured rock. The colour bar represents water saturation from 0 – 1.0.

Figure 9. a) White's model predictions of bulk modulus versus Sw at different frequencies (using a constant patch size of 0.5 mm). b) Corresponding effective fluid bulk modulus calculated from Figure 7a using Gassmann's equation.

Figure 10. Model fit to experimental trend for a) the 90^o fractured rock b) the 45^o fractured rock.

Figure 11. Model predictions for V_P/V_s ratios versus S_w for wave propagation a) parallel to the fractures (90^o to the fracture normal) b) the 45^o to the fractures.

Figure 12. Model predictions for V_P/V_s normalized by dry values versus S_w perpendicular (0^o to the fracture normal), 45^o, and parallel to the fractures (90^o to the fracture normal)

Figure 13. Model comparisons of V_P/V_s versus S_w ratios using a gas patch size of 2 mm in White's model for a) the blank rock b) the 90^o fractured rock.

Figure 14. a) Model comparison of V_P/V_s versus S_w ratios for the 45^o fractured sample using a gas patch size of 2 mm in White's model. b) Model fit to experimental SWS trend for the 45^o fractured rock using a gas patch size of 2 mm for the background rock saturation and the mixing law of Brie et al. (1995) for the fractured rock.

Figure 15. Model predictions (from Figures 13 and 14) for V_P/V_{s1} versus V_P/V_{s2} at 45^o and parallel to the fractures (90^o to the fracture normal). The colour bar represents water saturation from 0 – 1.0.

FIGURES

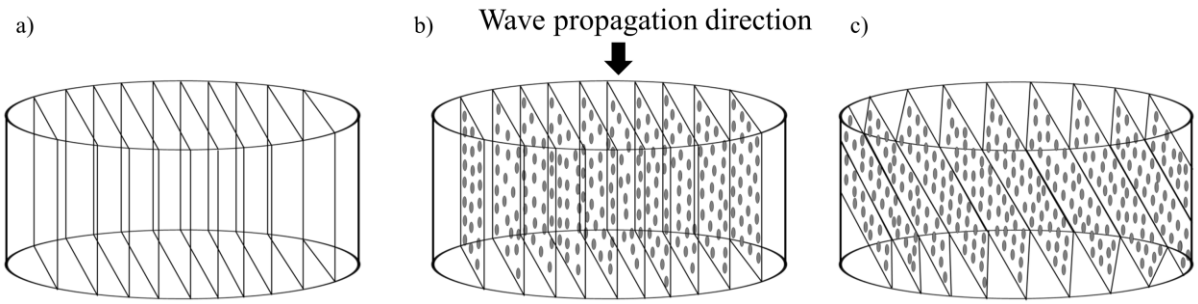

Figure 1. Schematic showing the orientation of a) layering in the blank rock, fracture planes for the b) 90^{o} degree fractured sample and c) the 45^{o} degree fractured sample, relative to the direction of wave propagation.

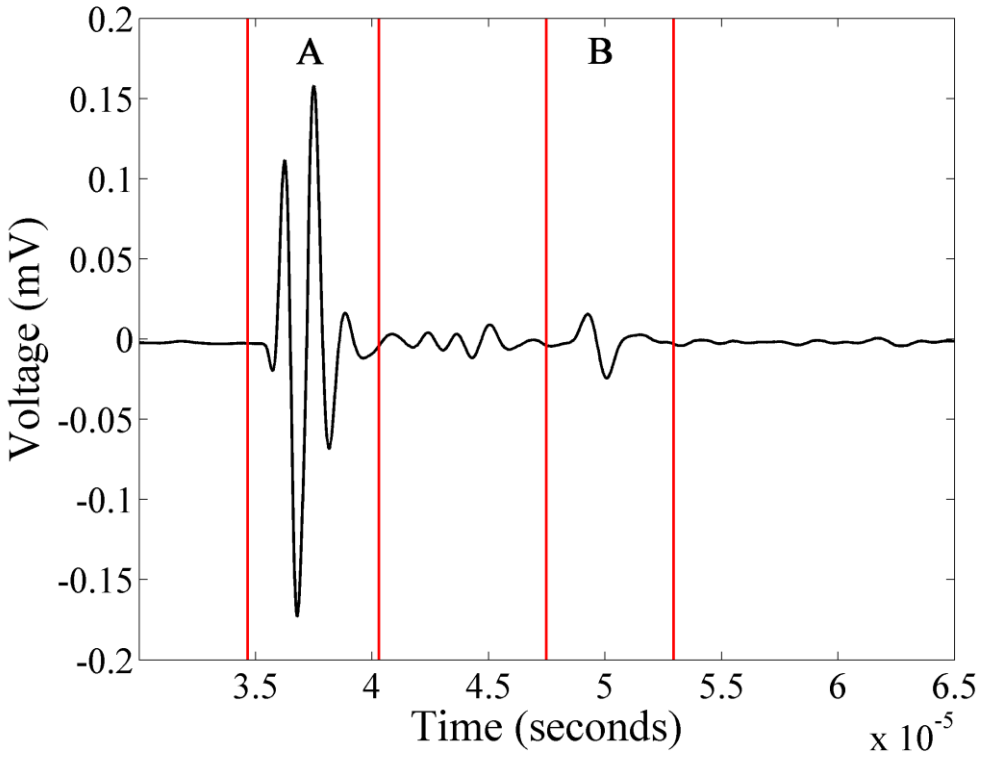

Figure 2. Typical P-waveform for the 45^{o} sample showing reflections from (a) the top of the rock (window A) (b) the base of the rock (window B), clearly separated by reflections of significant amplitude from within the rock sample.

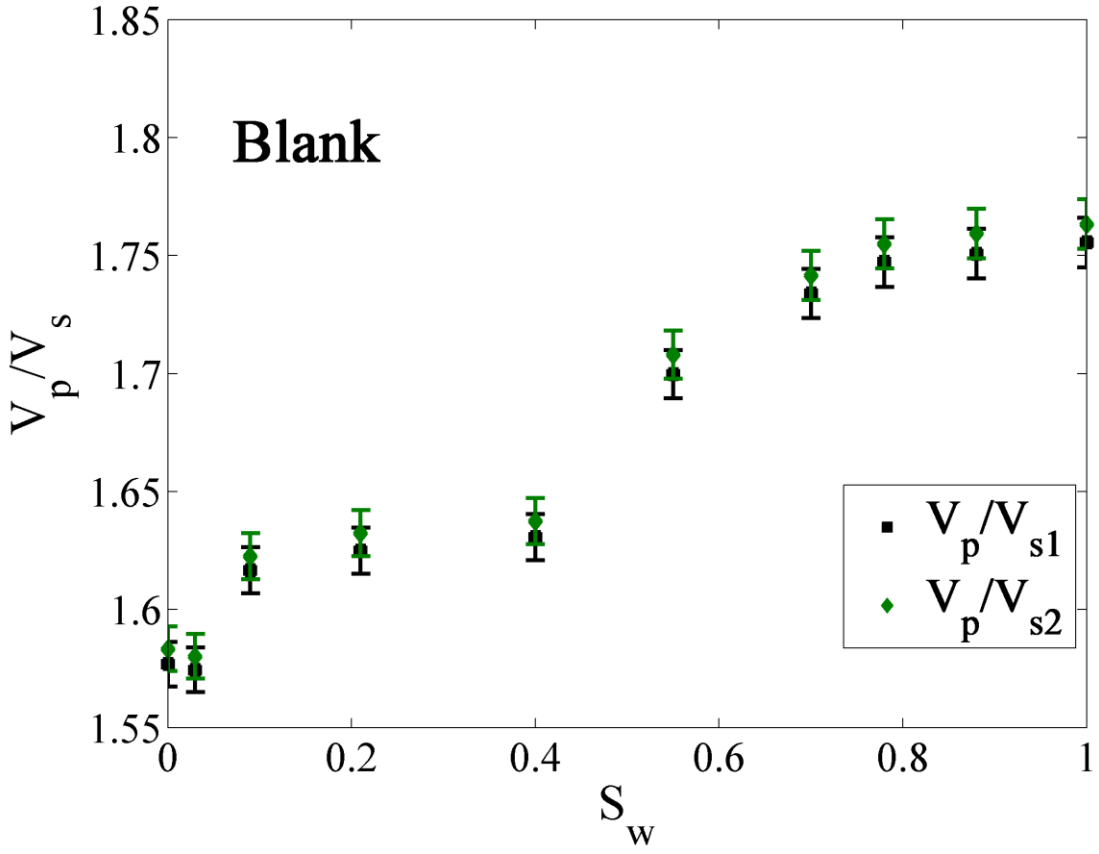

Figure 3. V_P/V_s versus S_w ratios for the blank rock (both fast S1 and slow S2 wave results are shown).

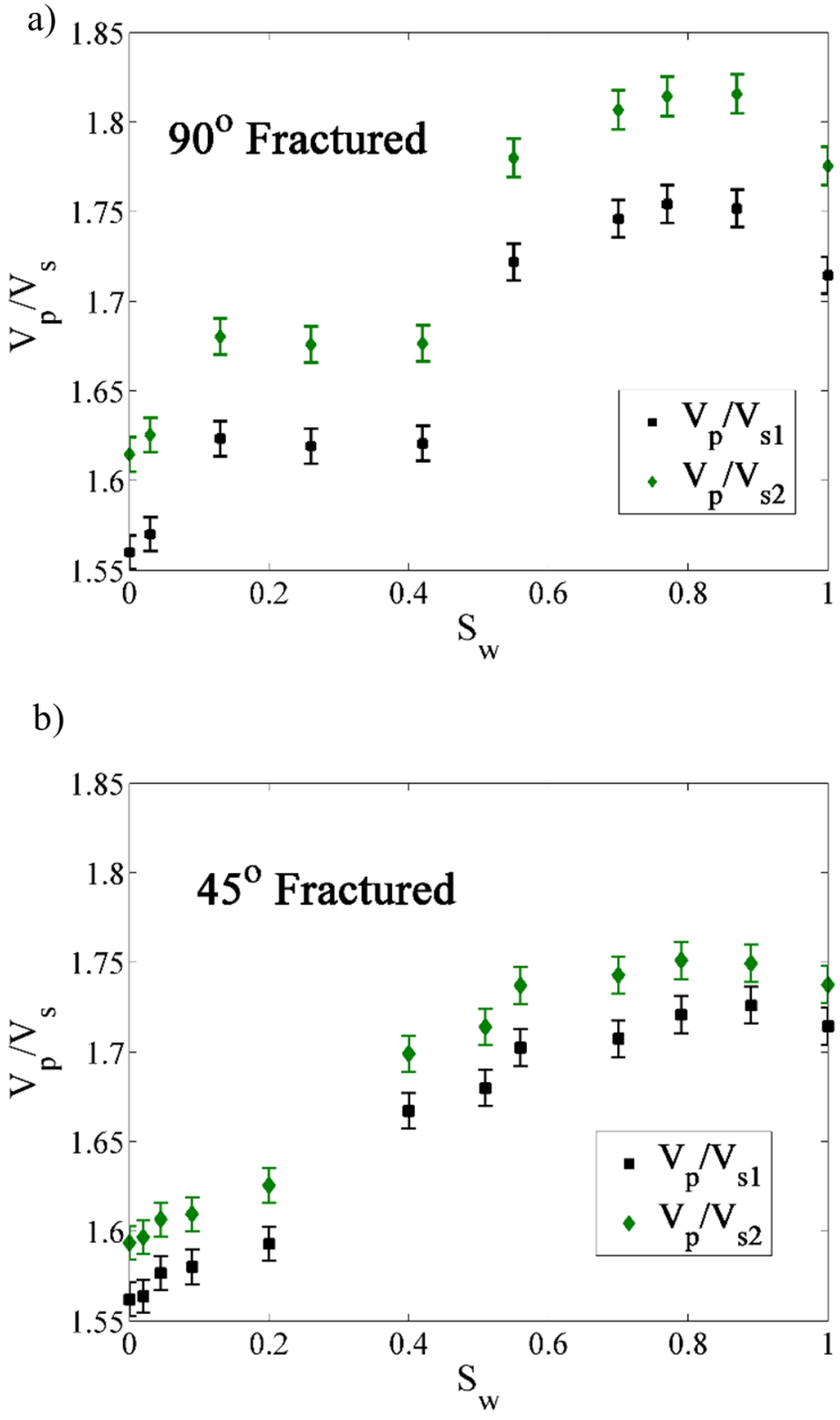

Figure 4. V_P/V_s versus S_w ratios for a) the 90° fractured rock b) the 45° fractured rock. Both fast S1 and slow S2 wave results are shown.

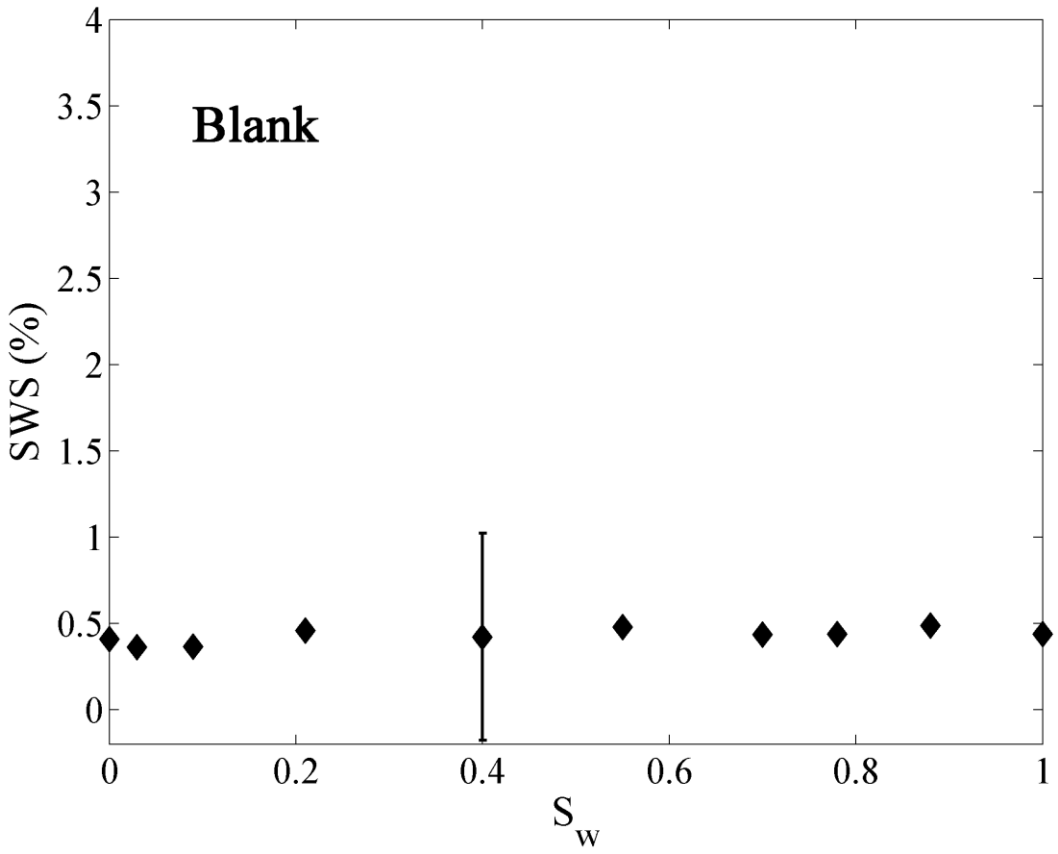

Figure 5. SWS versus S_w for the blank rock. Vertical error bar included.

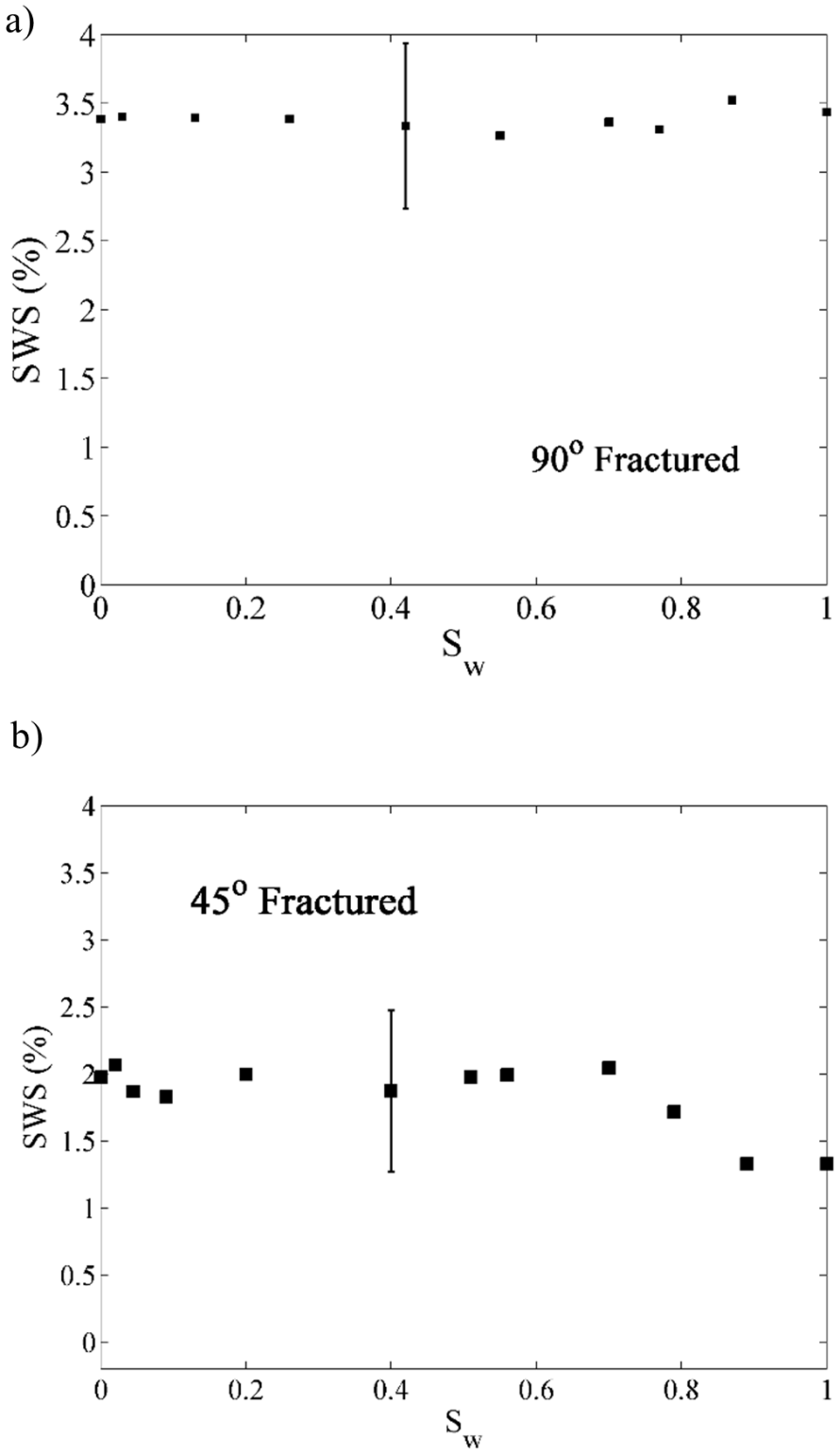

Figure 6. SWS versus S_w for a) the 90° fractured rock b) the 45° fractured rock. Vertical error bar included.

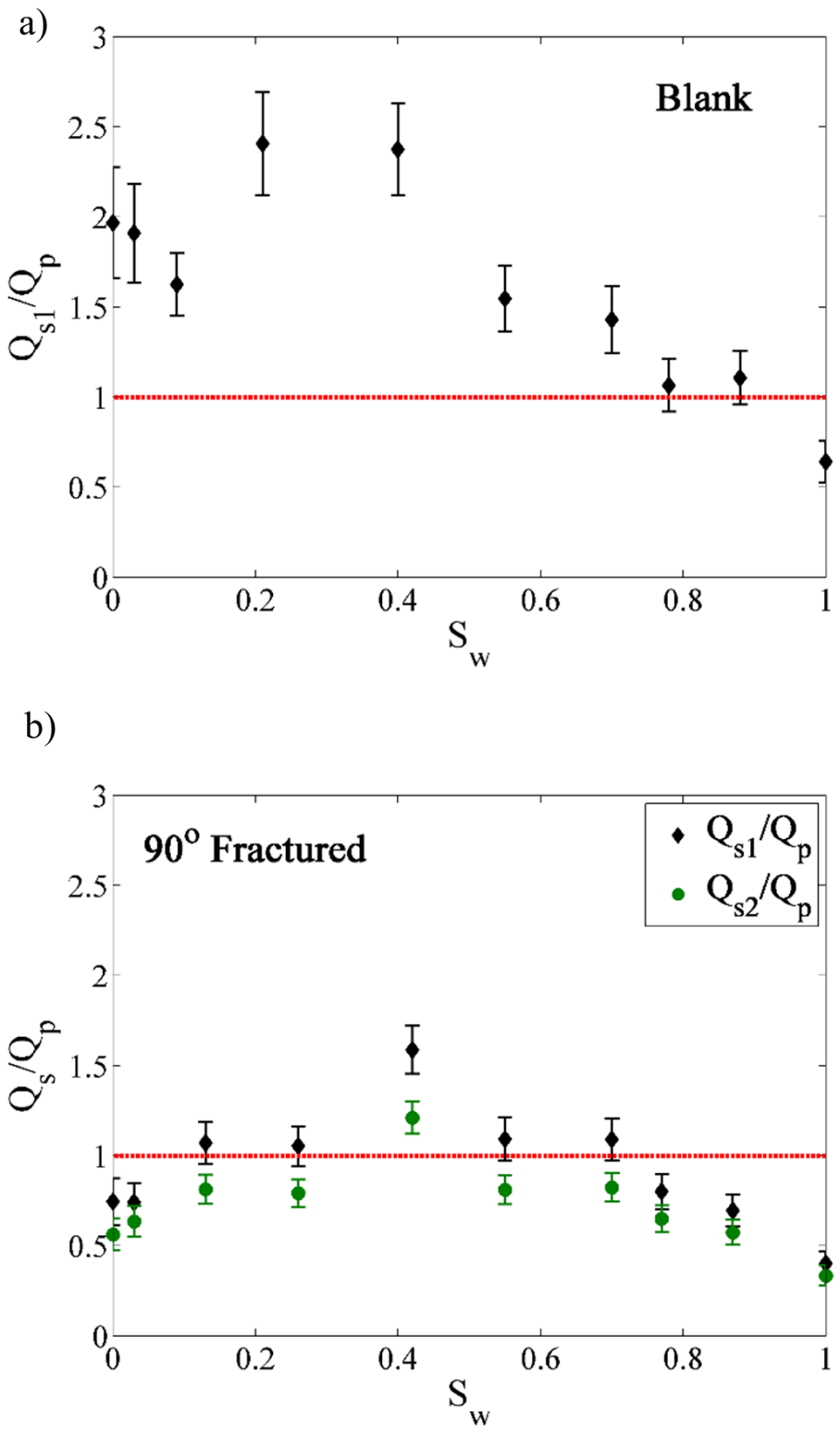

Figure 7. Q_s/Q_p versus S_w for a) the blank rock b) the 90° fractured rock.

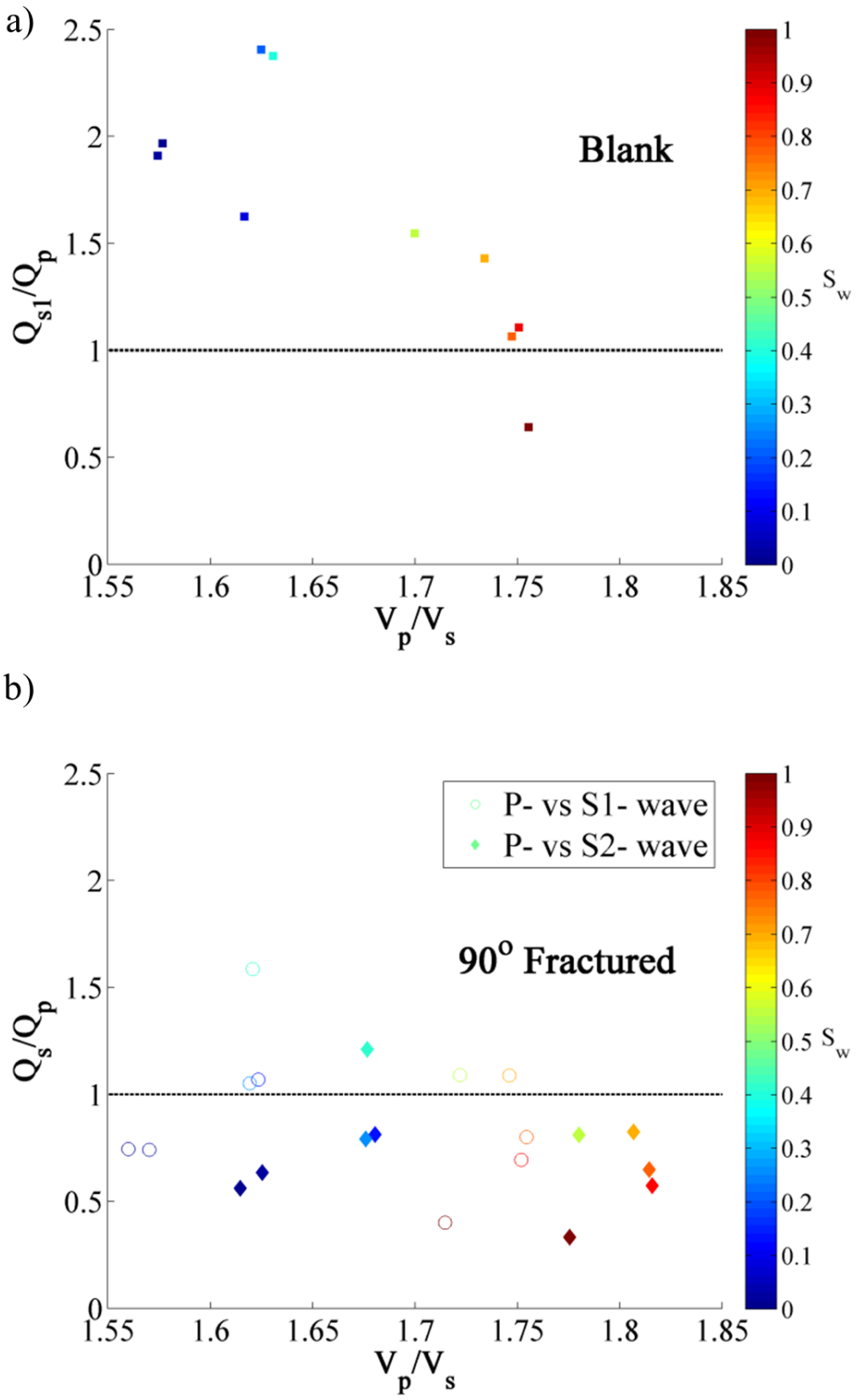

Figure 8. Q_s/Q_p versus V_p/V_s ratios at different saturation values for a) the blank rock b) the 90° fractured rock. The colour bar represents water saturation from 0 – 1.0.

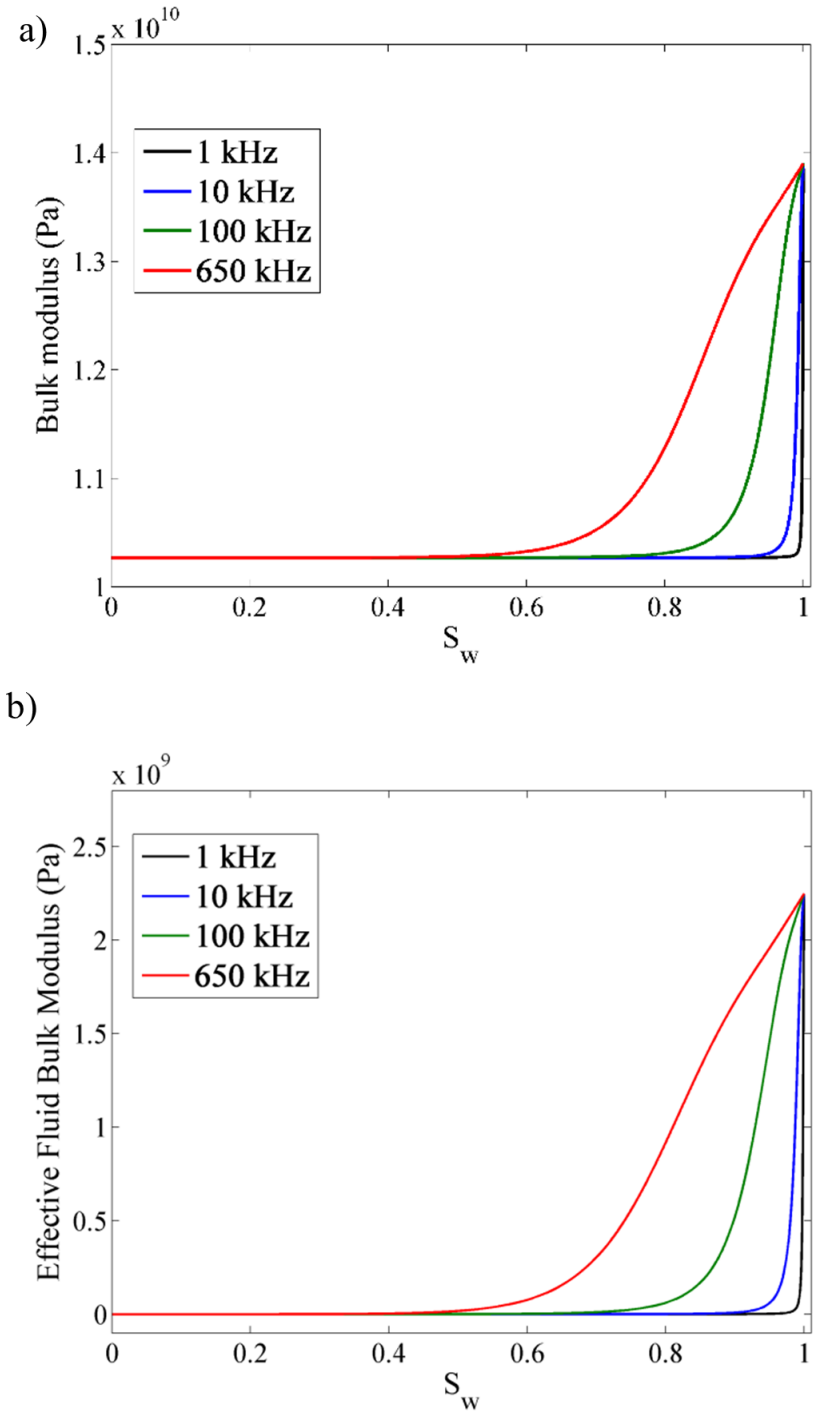

Figure 9. a) White's model predictions of bulk modulus versus Sw at different frequencies (using a constant patch size of 0.5 mm). b) Corresponding effective fluid bulk modulus calculated from Figure 7a using Gassmann's equation.

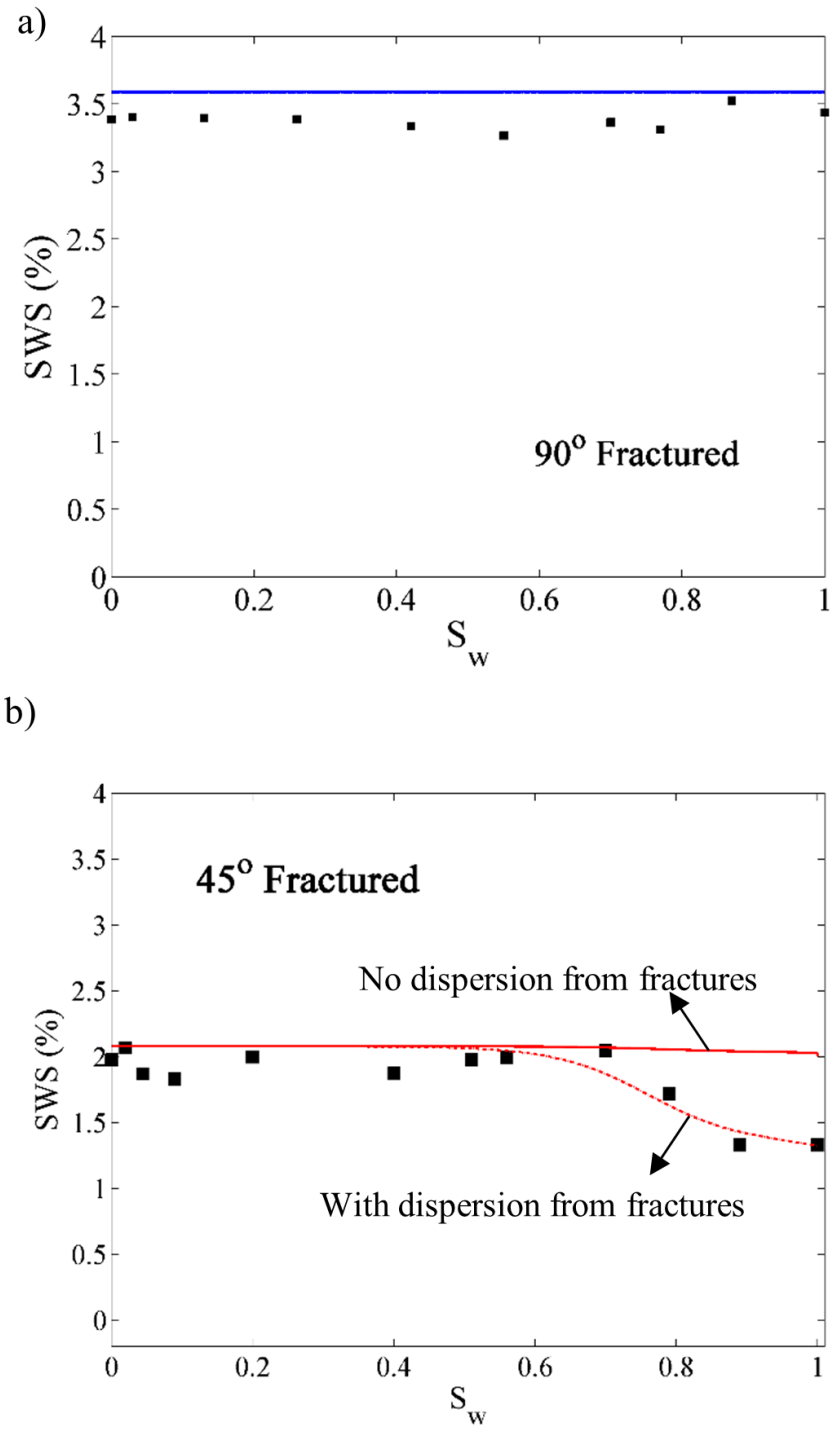

Figure 10. Model fit to experimental trend for a) the 90° fractured rock b) the 45° fractured rock.

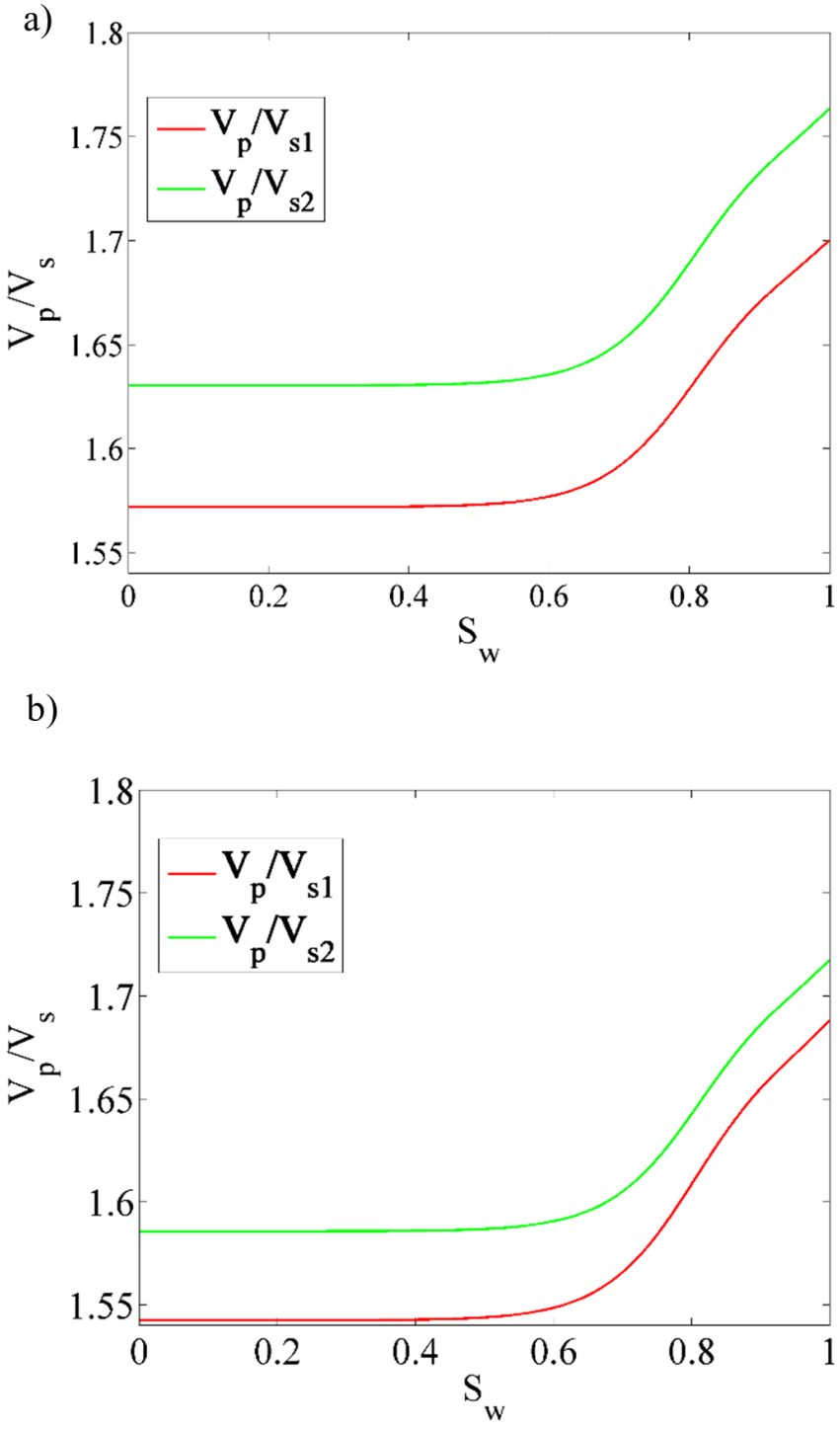

Figure 11. Model predictions for V_P/V_s ratios versus S_w for wave propagation a) parallel to the fractures (90° to the fracture normal) b) the 45° to the fractures.

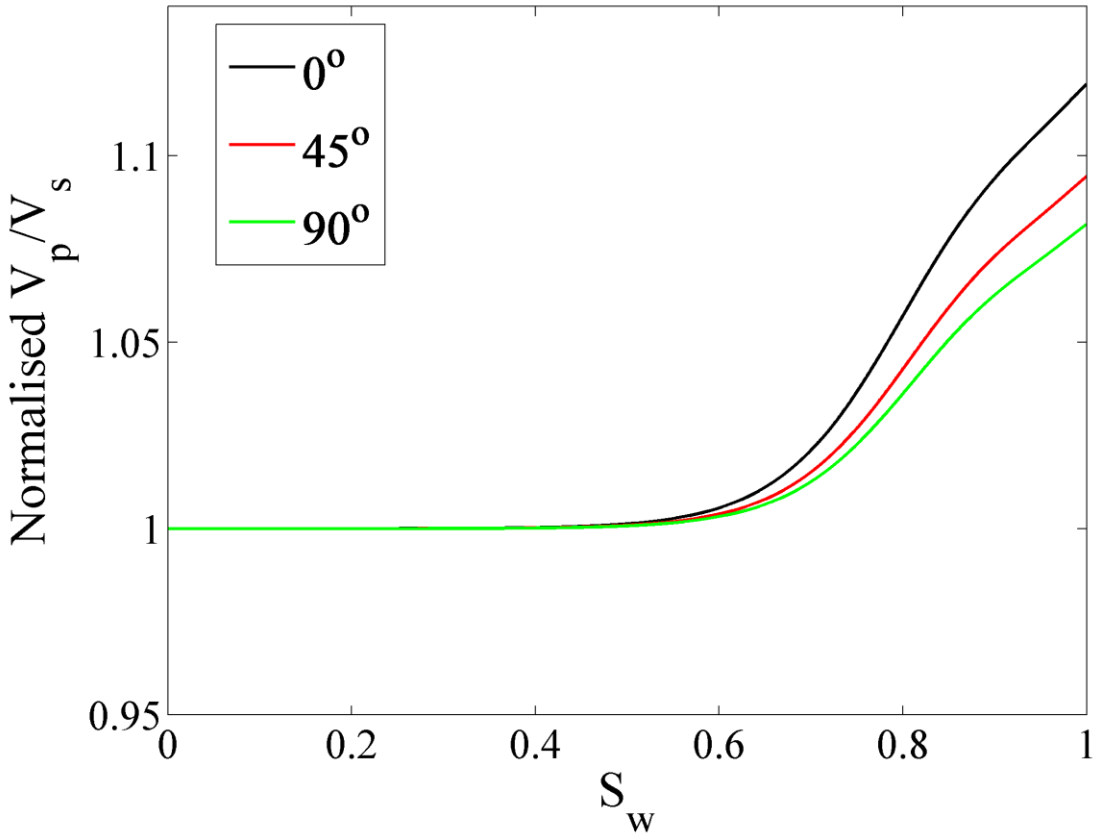

Figure 12. Model predictions for V_P/V_s normalized by dry values versus S_w perpendicular (0^o to the fracture normal), 45^o, and parallel to the fractures (90^o to the fracture normal)

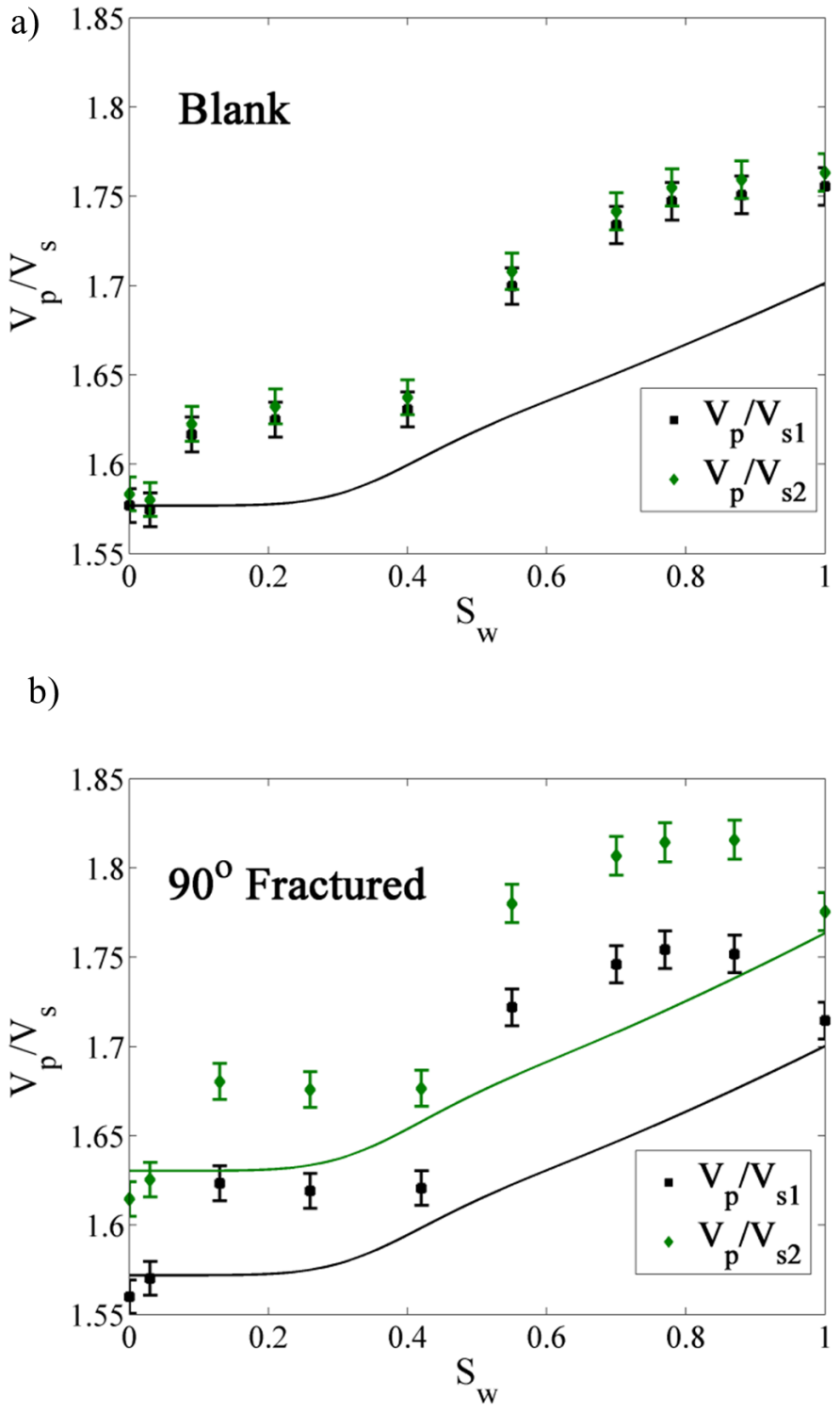

Figure 13. Model comparisons of V_P/V_s versus S_w ratios using a gas patch size of 2 mm in White's model for a) the blank rock b) the 90° fractured rock.

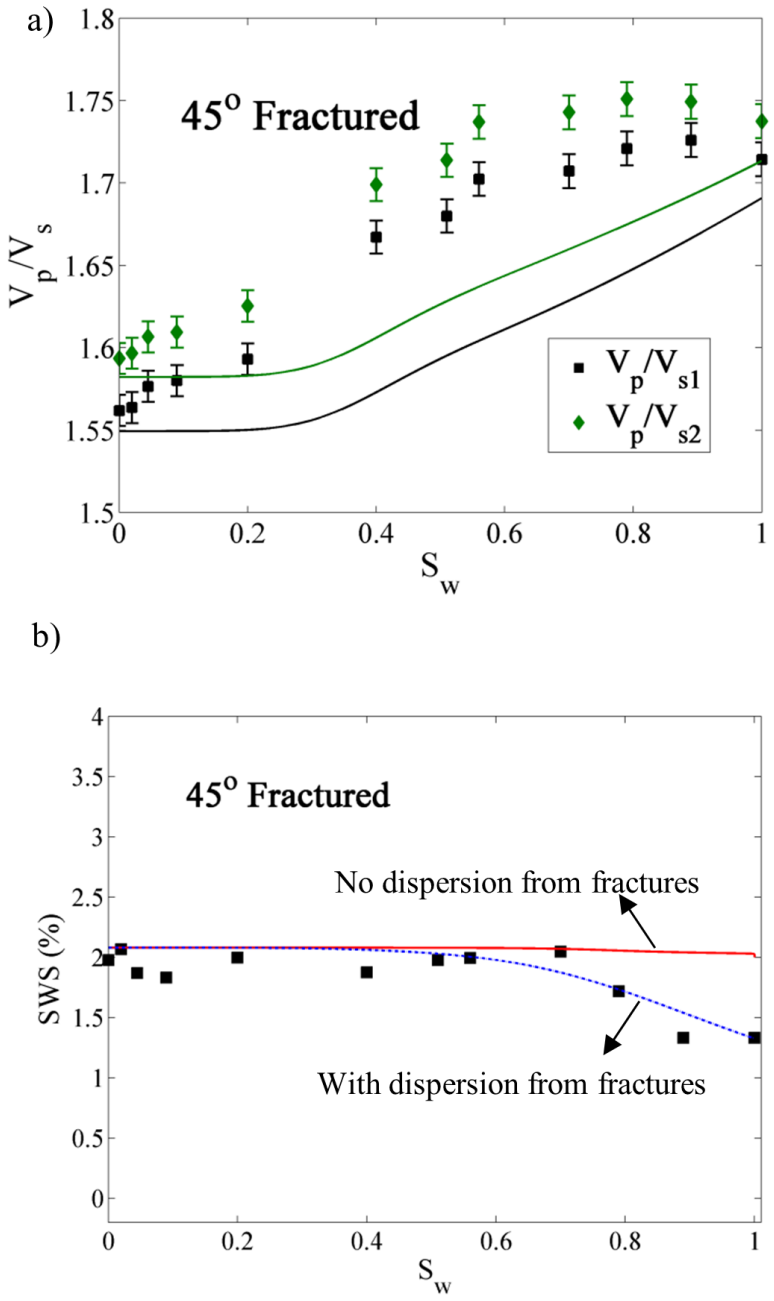

Figure 14. a) Model comparison of V_P/V_s versus S_w ratios for the 45° fractured sample using a gas patch size of 2 mm in White's model. b) Model fit to experimental SWS trend for the 45° fractured rock using a gas patch size of 2 mm for the background rock saturation and the mixing law of Brie et al. (1995) for the fractured rock.

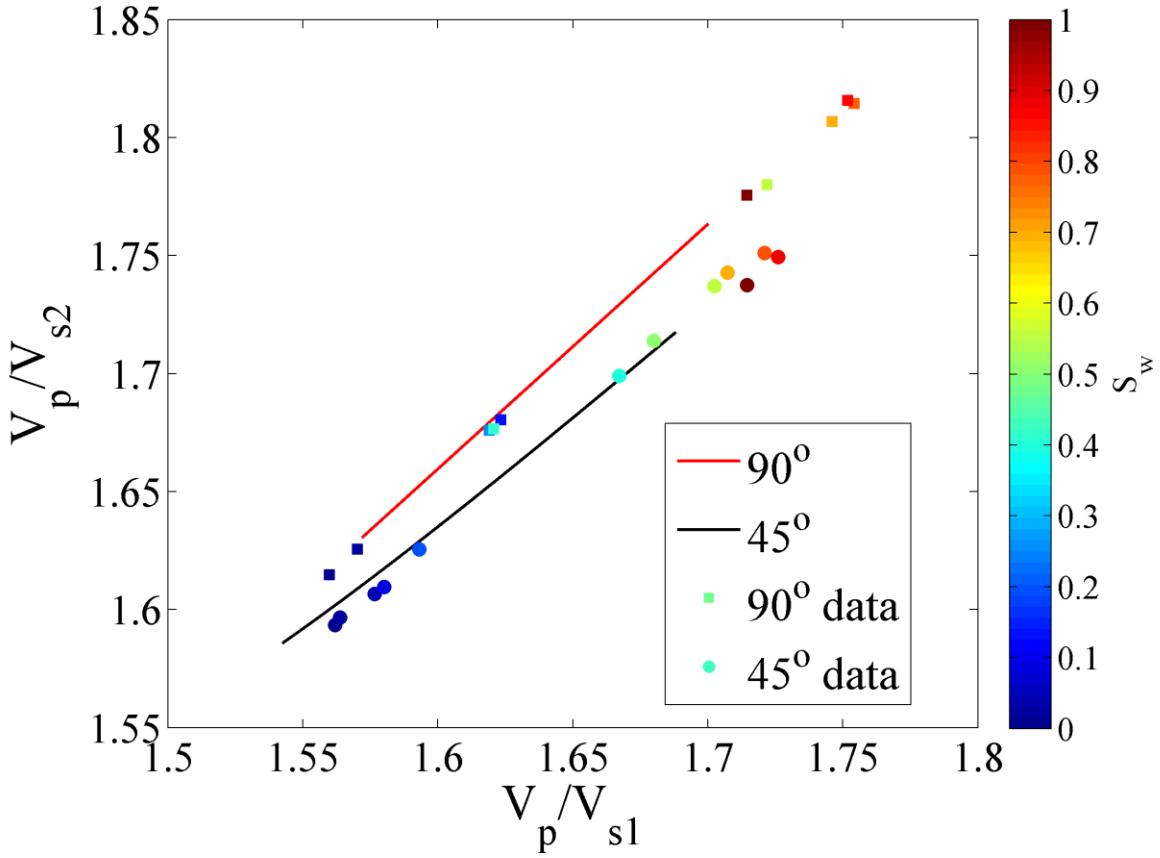

Figure 15. Model predictions (from Figures 13 and 14) for V_P/V_{s1} versus V_P/V_{s2} at 45° and parallel to the fractures (90° to the fracture normal). The colour bar represents water saturation from 0 – 1.0.